Developmental analysis of the cone photoreceptor-less little skate retina

Chetan C. Rangachar[1], Denice D. Moran[2], and Mark M. Emerson [1,2,3]

[1] Department of Biology, The City College of New York, City University of New York, New York, NY 10031, USA.

[2] Biology PhD Program, Graduate Center, City University of New York, New York, NY, 10016

[3] Biochemistry PhD Program, Graduate Center, City University of New York, New York, NY, 10016

Corresponding Author:

Mark Emerson, PhD.
Dept. of Biology
The City College of New York
The City University of New York
85 Saint Nicholas Terrace
New York, NY 10031
Email: memerson@ccny.cuny.edu
Ph: (212)-650-8417

Key Words: Retina, Photoreceptors, Rods, Cones, Skate, Development

Abstract

The retinal development of elasmobranchs--the superclass comprising sharks, skates and rays--is a poorly understood phenomenon. The clade is diverse in retinal phenotypes, with many sharks and rays possessing rods and multiple cone types. In contrast, the little skate (*Leucoraja erinacea*) has only a single type of rod photoreceptor, which is reported to have taken on some physiological and anatomical properties of cones. How does the little skate develop this photoreceptor system? To investigate this question, we identified an early stage of embryonic photoreceptor formation based on Otx2 expression. To assess whether cone photoreceptor gene regulatory networks regulated by the Onecut1 transcription factor were intact we developed an electroporation approach. Activation of a Onecut1-dependent reporter was not detected supporting a change in early Onecut1-transcriptional networks associated with cone photoreceptor formation. To assess developmental changes in gene expression, bulk RNA-Seq samples of embryos, juvenile hatchlings and adult retinas were generated. As expected, gene expression changes associated with cone photoreceptors of other species were not identified in the little skate and several cone-enriched genes were found to be pseudogenes. A splice isoform of Onecut1 with an additional 48 amino acid sequence located between the CUT and Homeodomain DNA-binding domains – referred to as "spacer isoform" or LSOC1X2 was identified and exhibited high expression in the embryo compared to juvenile and adult stages. To test if this LSOC1X2 isoform retained its regulatory potential compared to the isoform without the additional sequence, we tested it in a mouse retina reporter assay. Both skate Onecut1 isoforms were able to activate the Onecut1-dependent transcriptional reporter. Thus, the spacer isoform represents a developmentally regulated, novel retinal Onecut1 isoform with regulatory potential. This identifies it as a target for further analysis in the retinal development of the little skate and its elasmobranch relatives.

Introduction

Evolutionary Conservation of Photoreceptor Subtypes in the Vertebrate Retina

The retina exhibits a remarkable degree of structural conservation across the vertebrate subphylum. A recent meta-analysis of single cell retinal transcriptomes across a diverse set of vertebrates has shown that the main cell classes are universally conserved, with variation within cell classes arising from diverse evolutionary pressures[1]. There are six neuronal cell classes in the mature vertebrate retina: rod photoreceptors, cone photoreceptors, bipolar cells, horizontal cells, amacrine cells and ganglion cells, as well as one resident glial class, the muller glia[2]. Phototransduction, the process by which light is converted into neural stimulus, is accomplished by photoreceptors, which are of two types: rods and cones. Rods enable dim-light or scotopic vision, and cones bright-light or photopic vision. Mechanistically, these discrete roles are accomplished by binary differences in photon sensitivity and photopigment recycling kinetics: cones are less sensitive to light and their kinetics are faster, while rods are more sensitive and regenerate receptive photopigment slower. This allows cones to translate luminance differences in bright light fields into signal over noise, whereas the same conditions cause rod cells to be saturated. On the other hand, rods can detect very dim light, even single photons, in dark backgrounds, because the system leverages fewer photons into greater response, and in these conditions cones aren't sensitive enough to amplify to the point of perception[3]. Unlike rods, cones come in several subtypes, defined by the presence of opsins that specify different wavelength sensitivities. Many old world primates, like humans, possess three cone types: long wave-sensitive (red), medium wave-sensitive (green) and short wave-sensitive (blue)[4]. Some species, like the chick, possess ultraviolet-sensitive cones. Wavelength sensitive opsins mediate

color vision in species that have them. Rods on the other hand express only one type of opsin, rhodopsin, which has broad sensitivity peaking at ~500 nm[4,5].

Debate has existed for some time as to which of the two photoreceptor types--rods or cones--are the vertebrate ancestral photoreceptor. Species of jawless vertebrates or agnathans--in particular the lamprey, which diverged from the jawed vertebrates more than 500 million years ago--possess single-photon sensitive, cone-morphological cells [6]. Their photoreceptor type blurs the functional rod/cone distinction, but for our purposes, we will make the distinction based on morphology: rods have long cylindrical outer segments with enclosed lamellae (cytosolic disks where phototransduction occurs), and cones have shorter, cone shaped outer segments with lamellae continuous with the plasma membrane. By this definition, there is growing consensus that the ancestral vertebrate photoreceptor was a cone which, like rods, was sensitive to individual photons of light.

The relatively understudied chondrichthyans, or cartilaginous fishes—which diverged from the lineage leading to humans (bony fishes, or osteichthyes) around 450 million years ago—represent an important missing piece in the puzzle of vertebrate retinal development[7]. There are only two extant classes of chondrichthyes: holocephalans and elasmobranchs. The only extant order of the holocephalans are the chimeras and the elasmobranchs comprise all sharks, skates and rays. The chimera elephant shark (*Callorhinchus milli*) has three cone types, suggesting that the ancestral chondrichthyes retina had at least three cone types as well. However, elasmobranchs are diverse in the number and types of cone photoreceptors they contain. Most modern sharks (selachimorpha) have one cone type, and most stingrays (myliobaitoformes) have two. The unique little skate (*Leucoraja Erinacea*), a rajiform, has no

cone photoreceptors, only one type of rod photoreceptor. This suggests that various degrees of cone loss across the elasmobranch clade result from evolutionary pressure[8].

How did the little skate lose its cones? Firstly, it is notable that its single rod photoreceptor is, like all rods, sensitive to individual photons in the dark adapted state. However, uniquely, its rods have the ability to speed up their reaction kinetics in bright backgrounds, allowing for photopic response after a period of light adaptation. This means that the little skate's rod has two discrete modes of response: one rod-like, and one cone-like[5]. This kind of light adaptation is apparently unique among studied models to the little skate and its sister species, the winter skate. It also has been reported that structurally, the skate rod synapse has some features in common with cones including large invaginations at the tripartite synapse, multiple ribbons at single invaginations, and long telodendria[9]. This suggests that to accomplish their unique system of vision, they may have acquired some morphological properties of cone synapses. How this is reflected in early development--how genetic programs involved in cone specification in the skate's cone-bearing relatives have been repurposed or abandoned during skate retinal development--is a key outstanding question.

In this study, we explored the developmental dynamics of retinal formation and gene expression during little skate retinogenesis. We used histological examination of the embryonic retina to roughly define the period of photoreceptor formation through expression of Otx2 as well as cell cycle examination. Based on this analysis we created bulk RNA-sequencing datasets across three developmental stages—embryonic, hatchling, and adult—to identify transcriptional trajectories associated with photoreceptor fate decisions. This revealed initially high but declining expression of Onecut1, a key cone photoreceptor regulatory gene, alongside initially low but increasing expression of rod-associated developmental markers. Markers of rod

phototransduction increase in expression from embryogenesis to hatching, maintaining high expression in adulthood while examined cone phototransduction genes were not expressed and present with evidence of mutation. Molecular analysis of the cone-associated gene Onecut1 identified a developmentally regulated, alternative splice isoform. Finally, we assessed the functional consequences of this splicing event by modeling protein–DNA interactions with AlphaFold3 and validating the isoforms' functional activity by testing their ability to activate a well-characterized enhancer in retinal explants.

Results

Cell Cycle Dynamics of the Little Skate Retina

We initiated this study by examining the embryo stages of the little skate to determine the early stages of photoreceptor formation and to roughly characterize the cell cycle dynamics at this time, primarily to inform the implementation of electroporation (see below). During embryogenesis, little skates inhabit waters no warmer than 20°C, and the period from oviposition to hatching is approximately 20 weeks. These conditions could suggest that cell cycle turnover would be slower in this species than in models like the mouse (20 day gestation at 37°C) and chick (21 day incubation at 37°C). We chose to examine stage 50 days post oviposition (dpo) embryos based on a preliminary assessment of Otx2 expression, an early photoreceptor-associated marker, at this stage. We injected live 50 dpo little skate embryo yolks with thymidine analog 5'-ethynyl-2'-deoxyuridine (EdU), exposing several groups of specimens to the label for different lengths of time, and then embryos were fixed and analyzed for the percentage of actively dividing cells─identified by expression of mitosis marker phosphohistone H3 (PHH3)─that incorporated the EdU label at each time interval. Initial choices of incubation

window were broad, from 2 to 48 hours (Fig 1A-E, Fig S1). However, it was observed that at 4 hours, almost none of the PHH3+ population is EdU+ (1/87 counted cells across four specimens), and by 8 hours, over 70% of the PHH3+ population is EdU+ (43/56 counted cells across four specimens) (Fig 1F, S1A). Cells sensitive to uptake of EdU are within the S-phase and begin to express PHH3 as mitosis begins. The shortest time to incorporate the label in the mitotic population is a conservative estimate of the length of G2, the period between the end of DNA synthesis and cell division. Young (1985) performed more elaborate experiments in the P1 mouse with a similar methodology, using H3 thymidine as the DNA replication marker, and visual inspection of micrographs to label cells undergoing mitosis. Estimates from this experiment reveal that in the P1 mouse, the average length of G2 is 2.6 hours, and the whole cell cycle is 30 hours in length[10]. If we assume cell cycle dynamics in the skate are proportional, then the whole cell cycle length for dividing cells in the embryonic little skate retina is, conservatively, 46 hours. This time frame suggests that a three day culture should be more than sufficient to read out phenotypic effects of exogenous plasmids, which are believed to be incorporated into the nucleus after the breakdown of the nuclear envelope in prophase of mitosis.

In other vertebrates, such as the mouse and chick, photoreceptor-competent restricted retinal progenitor cells express Otx2, so we analyzed the presence of this developmental marker in the little skate's dividing (EdU+) population[11]. A small population of Otx2+ cells are present within this population post 4 hours incubation with EdU, which suggests that this developmental stage of skate could be undergoing photoreceptor neurogenesis (Fig 1B). In other vertebrate species, co-expression of Otx2 and Onecut1 in restricted RPCs present in the early embryonic retina and associated with cone formation, activates the cis-regulatory element ThrbCRM1[11]. At

more mature developmental stages, Onecut1 is no longer expressed in RPCs and rods, but not cones, are formed during this period[11,12]. A significant outstanding question then is whether or not the skate's Otx2+ dividing population expresses Onecut1, or if loss of Onecut1 expression could be a causal driver of the loss of cones in the little skate. We attempted to use a monoclonal antibody which recognizes mouse Onecut1 with high specificity, but we did not detect interpretable signal, most likely because it was raised against an epitope at the N-terminus of the mouse protein, which exhibits higher interspecies variation than the well conserved DNA binding domains (see Fig. 5).

To use a functional assay to determine if Onecut1 and Otx2 were co-expressed, we developed an electroporation-based assay. We adopted parameters developed for the marine organism *Ciona intestinalis*[13]. To test the electroporation procedure, retinas from 50 dpo embryos were electroporated with GFP and mCherry fluorescent reporters, both driven by the broadly active CAG element[14]. Wholemount visualization of the retina showed broad co-expression of the two fluorescent reporters, confirmed by confocal analysis of sections (Fig 1 G-K). The ThrbCRM1 element is co-regulated by Onecut1 and Otx2 and evidence suggests that both factors are required for reporter expression. We thus co-electroporated a ThrbCRM1::GFP reporter with CAG::mCherry to test for the co-expression of these two factors. However, in the electroporated portion of the retina marked by mCherry, we did not detect any GFP signal (N=3 retina) (Fig 1 L,M). This supports the hypothesis that Onecut1 may not be co-expressed with Otx2 during the early phases of photoreceptor formation of the embryonic little skate.

Bulk RNA-seq Reveals Robust Onecut1 Expression in Early Development, with Rod Program Genes Increasing in Expression in Later Development and Maturity

To examine gene expression broadly across little skate retinal development, we conducted bulk RNA sequencing of the whole retina. Eight specimens of three stages of little skate--three 50 dpo embryos, three hatchlings (P0), and two adults were analyzed. Gene expression was quantified after normalizing gene read counts to transcripts per million (TPM) across all samples (Fig 2A-C). Nr2e3 is an adult specific marker of rod photoreceptors with expression commencing in early rods and in the cone photoreceptors of some species[15–18]. We detected a relative minimum level at the 50 dpo stage, with stable high expression in the hatchling and adult (Fig 2A,C). The same trajectory is seen for the large Maf family members gene Mafaa and Mafb (Fig 2A,C). It is noteworthy that while Mafa is the rod specifying large Maf transcription factor in the chick, Mafb exhibits greater expression throughout development in the little skate, and as such may be the rod specifier in this species (Fig 2C, bottom)[19,20]. Nrl, the large Maf family member necessary for rod specification in the mouse, was not found in publicly available annotations of the little skate genome[21].

The complex developmental picture contrasts significantly with the expression trajectory of mature photoreceptor markers across these stages. For one, many differentiated cone markers, like cone transducin (Gnat2), arrestin (Arr3), and phosphodiesterase (Pde6c), are not present in the little skate genome; at least in their evolutionarily conserved locations. The chimera elephant shark, a distant chondrichthyes relative of the little skate, possesses three types of cone opsins--Rh2, Lws1, and Lws2--as well as cone transducin, phosphodiesterase subunit 6c and arrestin[8,22] (Fig 2D). In the elephant shark, these genes are all present in chromosomal loci which have conserved syntenic structure with several, if not all, elasmobranchs (Fig S1B). To see how these genes have been preserved or modified among the elasmobranchs, we inspected the conserved genomic loci for these genes across three species. The catshark was used as a representative

selachimorph (modern sharks), the devil ray the representative myliobatiform (stingrays), and the little skate a representative rajiform (skates). The catshark was selected because it is one of the most extensively studied elasmobranchs, and reports have characterized it as rod-exclusive, or nearly exclusive[23]. The devil ray was chosen because it is a closer relative to the skate, and as a myliobatiform with genes for short wave-sensitive and long wave-sensitive opsins, likely has cones[24]. The devil ray is also predicted to splice Onecut1 in a similar manner to that which we observe directly in the little skate, as we will discuss.

The chromosomal position of cone arrestin (arr3), transducin (gnat2), and phosphodiesterase subunit 6c were visualized using NCBI's Genome Data Viewer in each of these species. For each of these genes, the flanking genes, or those annotated nearest upstream the 5' start site and nearest downstream the 3' terminus of the elephant shark cone gene, were in conserved positions for all species. As such, we extracted the entire genomic sequence in between the flanking genes for each species and analyzed conservation of this genome sequence relative to the elephant shark protein coding sequence using TBLASTN. The program scans for all possible reading frames within an extended region which will result in an amino acid sequence aligning to that of the elephant shark. The little skate genome sequence shows significant alignment for each of these three genes (Fig S2). In multiple cases a nonsense mutation in a conserved region results in the single base conversion of a glutamate (GAA, or GAG) to a STOP (TAA, TAG or TGA). This suggests that they have become vestigial by accumulation of nonsense mutations. Consistent flanking genes were not available for the three elephant shark opsin genes, rh2, lws1, and lws2.

Cone specific cyclic nucleotide gated channel (CNG), cnga3, is present in the genome without nonsense mutations, however it does not increase in expression from embryo to

adulthood (Fig 2B). This aligns with the idea that it is dispensable for vision in this organism as it would be expected to increase as cone cells differentiate as development progresses. In contrast, rod CNG, cnga1, rod arrestin (s-arrestin), rod phosphodiesterases (pde6a/b), rod transducin (gnat1), and rhodopsin all exhibit the same expression trajectory: low embryonic levels, and high levels of expression in the hatchling and adult (Fig 2B).

The expression of onecut1 was examined to test the hypothesis that the lack of cone photoreceptors generated in the little skate could be due to a change in the cis-regulation of Onecut1 that prevented its expression in RPCs with Otx2 during early photoreceptor formation. The bulk RNA-Seq dataset obviously does not reveal any tissue specificity for which cells would express Onecut1 but as the other cells that typically express Onecut1 such as horizontal cells and retinal ganglion cells make up a small number of the cells in the little skate retina, it could be hypothesized that the expression of Onecut1 would be lowly expressed and relatively steady if these were the only cells that expressed it. However, upon examination of the three studied stages, Onecut1 expression is highest by TPMs in the 50 dpo embryo. (Fig 2C, top) In mice and chicks, Onecut1 and Otx2 drives the expression of Thrb through the ThrbCRM1 element. Examination of Thrb expression also showed very low expression (0.214 TPM). (Fig S2C) This suggests that either Otx2 and Onecut1 are not expressed in the same cells, there has been a change in the cis-regulation of Thrb, and perhaps other cone genes as well, or that the Otx2/OC1 transcription factor activity could be compromised.

Little skate Onecut1 has two splice isoforms with developmental changes in ratio

To test if there could be differences in the Onecut1 gene expression in the little skate, we constructed an embryonic retinal cDNA library using oligo-dT primers to isolate mature transcripts from embryonic bulk RNA extracts. Primers specific to the region just outside the

Onecut1 coding sequence in untranslated sequence were used to PCR amplify Onecut1 transcripts. The recovered amplicon was sequenced and revealed to be skate Onecut1 through NCBI's nucleotide BLAST. However, there were two unexpected modifications to the gene as compared to the annotated reference sequence on the standard available reference genome (Leri_HHJ_1). First, we found a 366 bp deletion in the intrinsically disordered domain (IDR) of the protein, spanning the first two exons (Fig3A, B). This truncation maintained the open reading frame and did not interrupt either of oOnecut1's two DNA binding domains, the CUT and homeodomains. We inquired as to the possibility of this sequence deletion being an artifact of our library preparation, or downstream PCR, as opposed to real splice variation. To isolate reads from the bulk RNA sequencing experiment that contained information on this potential splice site, we subsetted the BAM reads aligning to Onecut1 from the embryonic samples to only those including a 10 base pair (bp) "query" truncation identifying sequence. Reads containing the 10 bp query sequence contain base information on the continuing downstream sequence. If reads with the query contained downstream bases that matched the sequence of the recovered truncated isoform, it would support that the truncation was either a natural occurrence, or that there was a more fundamental technical issue causing sequence deletion in both the bulk RNA-seq experiment *and* the cDNA library amplification. However, alignments with the truncated transcript were not observed: the downstream sequence of reads containing the 10 bp truncation query sequence experiment never aligned with the recovered isoform's truncated region (Fig S3D). As such, it is likely that the IDR truncation in the recovered onecut1 cDNA amplicon resulted from an artifact of the library synthesis or the following PCR amplification.

The second modification in the recovered transcript was a 144 base pair *insertion* between the DNA binding domains (Fig 3A, C). The CUT domain of Onecut1 ends at the 3' end

of exon 2, and the homeodomain begins at the 5' end of exon 3. The 144 base pair insertion corresponds to a region of the genome in the intron between these two exons (Fig 3B). It therefore represents real splicing variation of this gene, resulting in a new alternative exon which has not yet been annotated in this organism. The region encodes a 48 amino acid "spacer" in between the DNA binding domains that is predicted to be intrinsically disordered. An intrinsically disordered spacer between the DBDs is found to be alternatively spliced into the Onecut1 gene in the rat liver[25]. Pou family member genes are also observed to undergo alternative splicing to modify the linker sequence between DBDs, which can lead to changes in DNA binding sequence specificity[26]. Interestingly, a BLAST search of the sequence of the recovered skate Onecut1 transcript results in a top hit for the Onecut1 sequence of the lesser devil ray (*Mobula hypostoma*). The similarity arises because the annotation reference for the devil ray genome predicts a similar spacer coding sequence to be spliced into its mRNA transcript of Onecut1. It is of interest to explore the extent and purpose of this broad elasmobranch phenomenon, for visual development and otherwise.

We next investigated the possibility that the canonical Onecut1 isoform (the isoform without the spacer exon), may be co-expressed temporally with the spacer isoform in the little skate retina. Using the same bioinformatics method for validation of the truncation variant, we confirmed the presence of the spacer element in the RNA-seq FASTA reads. We used a 10 bp query sequence upstream of the inserted sequence and analyzed the downstream bases in reads containing the sequence. The 3 bases "CGT" identify the beginning of exon 3, and 3 bases "GGA" identify the beginning of the spacer exon. Interestingly, both the canonical splicing mode, wherein exon 2 splices directly into exon 3, and the novel "spacer" splicing mode,

wherein exon 2 splices into the alternative spacer exon, are accounted for at all studied stages (Fig 3C, D).

We next characterized the ratios of splice isoforms across the three studied stages. The 50 dpo embryo expresses significantly higher levels of Onecut1 in general (46.09 TPM, vs 25.28 TPM in the hatchling, and 6.67 TPM in the adult), but the ratio of transcript types in the embryo significantly favors the spacer isoform (68.42% spacer across all samples) (Fig S2C, S3A, 3D). However, there is lower relative abundance of the spacer isoform in bulk transcripts at the hatchling and adult stages (10% spacer across hatchling samples, 11% spacer across adult samples). Chi-squared analysis indicates that alternative splicing of the gene is stage-specific. As the canonical developmental role of Onecut1 in restricted RPCs/cones is to activate the Thrb and other cone genes, this finding begged the question of whether the inclusion of a long (48 amino acid) spacer element in between the DNA binding domains could possibly disturb this interaction[11,27]. As the cDNA library preparation amplified only the IDR truncated product, we synthesized full length gene fragments for little skate canonical Onecut1 (LSOC1X1), and little skate spacer Onecut1 (LSOC1X2), which is identical in sequence to the canonical transcript, with the inclusion of the 144 bp spacer. Gene fragments were synthesized with restriction enzyme sites at the 5' and 3' ends and cloned into expression vectors. The truncated product was also cloned and used in subsequent overexpression analysis to assess the effect of IDR deletion on skate Onecut1 transcriptional activity (Fig S4).

LSOC1X1 and LSOC1X2 Activate ThrbCRM1 in the P0 Mouse

To make a prediction of what the effect of the spacer exon inclusion would be, we first modeled the local interaction of the Onecut1 and Otx2 proteins with ThrbCRM1 using Alphafold3, which has recently been shown to model multiple molecular interactions to high

accuracy[28]. The control model included only the simplest assumptions: two molecules of mouse Otx2, one molecule of mouse Onecut1 and the ThrbCRM1 double helix. (Fig 4A, left) In this control, the limited assumptions generate a model which places the transcription factor DNA binding domains in contact with their known binding sequences from a whole-complex point of view. We replaced mouse Onecut1 in the model with the protein LSOC1X1, then with LSOC1X2 (Fig 4A). We considered that the inclusion of a spacer element might introduce steric constraints that prevent the normal binding mode at this element. However, it is suggested by the model that the predicted disordered spacer region does not cause significant enough disruption to the complex to favor a qualitatively different binding mode, at least with the parameters that we set. (Fig 4A, middle, right)

Table 1

Driver	Electroporation Control	Reporter	Antibody (AB) to detect onecut1	Drives thrbCRM1?
+ctrl pCAG:: mouse onecut1	pCAG::Bgal	thrbCRM1::GFP	Onecut1 B1	Yes
-ctrl pCAG::xxx	pCAG::Bgal	thrbCRM1::GFP	Onecut1 B1	No
pCAG:: LSOC1X1	pCAG::Bgal	thrbCRM1::GFP	Onecut1 B1	Yes

pCAG:: LSOC1X2	pCAG::Bgal	thrbCRM1::GFP	Onecut1 B1	Yes
pCAG:: LSOC1X2-Ndel	pCAG::Bgal	thrbCRM1::GFP	Onecut1 B1	No

To validate the functional activity of these isoforms, we performed ex-vivo electroporation of the Onecut1 isoforms with the ThrbCRM1::GFP reporter into the postnatal mouse retina. The introduction of canonical mouse Onecut1 in this paradigm leads to robust induction of the ThrbCRM1 reporter as endogenous cells targeted by electroporation at this timepoint do not express Onecut1 and do not activate the reporter. Furthermore, it was shown that this reporter activation depends on Otx2 using a Flox allele suggesting that the interaction/synergy of Onecut1 and Otx2 is revealed in this assay. The skoc1a and skoc1b isoforms were cloned into a CAG based misexpression vector which has broad activity in dividing cells and their progeny in the mammalian retina[29]. P0 retinas were electroporated in each of four groups: CAG :: mouse onecut1, CAG :: LSOC1X1, CAG :: LSOC1X2, and negative control CAG :: NULL). The CAG :: nuclear Beta-Galactosidase and the ThrbCRM1:: GFP reporter plasmid were co-electroporated as an electroporation control and OC1/Otx2 reporter, respectively. After two days of culture, retinas were processed for confocal microscopy to visualize electroporated cells (Bgal), the ThrbCRM1 reporter (GFP) and OC1 protein immunoreactivity. As expected, negative control retinas had no induced GFP reporter expression and no additional Onecut1 activity beyond that detectable in endogenous HCs (marked by arrows and unelectroporated) (Fig 4B). In contrast, mouse Onecut1 induced ThrbCRM1 reporter activity and led to a marked increase in OC1 immunoreactivity (Fig 4C). Interestingly, both LSOC1X1

and LSOC1X2 induce the expression of ThrbCRM1::GFP (Fig 4 D, E), but lack immunodetection by the Onecut1 antibody (Fig 4 D'', E''). The antibody result confirms that this reagent is not a good candidate for detecting endogenous LSOC1. It also shows that at a qualitative level that the skate OC1 protein is sufficiently conserved to activate the ThrbCRM1 element and also to coordinate this activation with endogenous mouse Otx2. Interestingly, at a qualitative level the spacer isoform is also able to activate the ThrbCRM1 element and thus the presence of the spacer amino acids does not interfere with this activity.

Discussion

The retina of the little skate presents a compelling model for understanding how evolutionary forces can reshape photoreceptor identity and developmental gene regulation. Although the canonical vertebrate retina comprises both rods and multiple cone subtypes, the skate retina is unusual in possessing only rods, yet retaining some capacity for photopic vision. Our results demonstrate that skates are amenable to developmental analysis of the retina which can answer some remaining questions about visual development in this species and elasmobranchs more broadly. This has the potential to significantly broaden our knowledge of genetic regulatory conservation in vertebrate retinal development.

In studied vertebrates, differentiation to retinal cell types from RPCs is a complex process which involves intrinsic cell factors (i.e. transcription factor markers of cell fate), extrinsic factors (i.e. notch signaling, cell-cell communication), and stochastic processes (i.e. distribution of internal factors). A common multipotent retinal progenitor cell is the ultimate source of all mature cell types. Birthdating experiments have revealed that cell types are born in temporally ordered but overlapping sequence[30]. Cone and rod genesis overlap, and progenitor/precursors of

these cell types require and express Otx2, but the gene regulatory mechanisms that direct these cells to unique fates are less clear. Lineage tracing for Olig2 expression, a marker for restricted RPCs, shows that these cells can generate clones of either cones or rods, but daughters of single olig2+ RPCs are not observed to comprise both rods and cones[31,32]. However, as we and others have seen, ectopic expression of determining factors of either rods or cones can induce at least partial fate-switching to the other cell type under these conditions. Ectopic Onecut1 can cause rod-fated RPCs to express genes associated with immature cones and directed expression of Nrl is sufficient to induce rod gene expression in developing mouse cones[11,33].

Onecut1 acts to both promote cone genesis and prevent rod genesis. There are several aligning genetic perturbation assays that underscore this gene's role in mutual exclusion. Onecut1 KO mice express greater transcript levels of Nrl, Onecut 1/2 double knockout mice have a significant reduction in cones and overexpression of Onecut1 fused to constitutive engrailed repressor element results in increased abundance of Mafa+ photoreceptors in chick[11,34]. Interestingly, the genetic regulatory elements that drive the specification of photoreceptors also have a role in the development and maintenance of the pancreas and liver. In the mouse pancreas, Onecut1 directly represses Mafa in developing islet B cells by preventing transcription factor Hnf3b, or Foxa2, from binding to an enhancer regulatory region upstream of the Mafa promoter[35]. In this context, Onecut1 is required for early development, but is downregulated as these cells mature, leading to upregulation of Mafa in mature B cells. In a diabetic mouse model, Onecut1 is overexpressed in mature B cells, which results in dysfunction of insulin production. Insulin supplementation decreases Onecut1+ cells, increases Mafa+ cells, and restores normal glycemic control. Thus the restriction of Onecut1 expression to early development, with

downregulation and an attendant large Maf family member upregulation in maturity, is a feature of characterized developmental systems.

In the rat liver, Onecut1 enhances expression of several developmental genes, such as Hnf3b and Ttr but has also been observed to repress glucocorticoid-regulated genes, such as Pfk-2 and Pepck[25,36]. The mechanism by which Onecut1 represses glucocorticoid-regulated genes has been elucidated: inactivation of the glucocorticoid response unit (GRU) by Onecut1 is mediated by an interaction between the glucocorticoid receptor DNA binding domain and the N-terminal half of the Onecut1 protein, which results in repression of the response element[21]. Two isoforms of Onecut1, analogous to those observed in the little skate retina, are expressed in the rat liver and mediate isoform-specific interactions at developmental and glucocorticoid-responsive promoters. In the rat, Onecut1 is alternatively spliced to include a 26-amino-acid spacer exon between the DBDs, as opposed to the 48-amino-acid spacer exon seen in the little skate retina. Intriguingly, these protein isoforms show differences in their binding to promoter elements, suggesting that this altered structure changes their DNA binding preference. In the rat liver, HNF6b exhibits greater binding affinity than HNF6a at the rat Hnf3b promoter[25]. Additionally, both HNF6a and HNF6b repress expression of the GRU for Pfk-2, but only the HNF6a isoform represses the GRU for Pepck. In fact, the GRU for Pepck is enhanced by overexpression of HNF6b through an unknown mechanism[36]. This differential selectivity suggests that alternative splicing of this gene may result in complex modulation of developmental programs. In this study, we reveal that the activity of the spacer isoform of skate Onecut1 demonstrates some redundant activity with the canonical isoform at the ThrbCRM1 element. The contrast between the regulation of Onecut1 in the skate retina and the retinas of better-studied vertebrates, which have

not been observed to alternatively splice Onecut1, seems likely to figure prominently in more complete models of the development of the skate's photopic-responsive rod photoreceptor.

The relationship between the skate Onecut1 isoforms and all the previously characterized Onecut1 responsive elements should firstly be demystified to assess how alternative splicing of this gene is involved, if at all, in the production of the little skate's rod-only retina. One hypothesis is that at early stages in development, Onecut1 is spliced in photoreceptor progenitors into the spacer isoform, permitting the formation of cone-like synapses without the irreversible commitment to cone identity that may accompany lone expression of the canonical isoform. Later in development, upon downregulation of Onecut1, rod outer segment formation is permitted to continue. This hypothetical model, where cone and rod programs instruct development within the same cells, but are activated by temporally distinct cues, would represent a significant departure from the vertebrate photoreceptor development paradigm, where rod and cone developmental pathways are delineated early, with robust mutual exclusion of the genetic determinants of cell type[32]. Such a scenario may have been necessary to acquire properties of light responsiveness that are apparently unique to this species.

Single cell experiments of the little skate retina will be useful to determine the cell-type specific expression of Onecut1 isoforms, and their relationship with photoreceptor development. In addition, sequencing data from a broader range of developmental time points will help to crystalize how stage specific splicing occurs, and how genetic programs are modulated depending on absolute and relative abundances of the two isoform types. These experiments will also allow for cell-type comparisons with transcriptomes of other elasmobranchs. Single cell analysis of the hatchling catshark was recently reported, and this study further supports previous reports that this species also has only rod photoreceptors[37]. Are the developmental mechanisms

that cause rod-exclusivity in this species similar to those that cause it in the skate? It should be noted that these species have diverged over the course of 286 million years, but chromosomal arrangement and gene order are well conserved across the chondrichthyans[22].

Studies of alternative splicing of Onecut1 in other elasmobranchs will also aid in our understanding of how and why this phenomenon evolved in the little skate. As noted, the initial BLAST search of the skate Onecut1 protein sequence recovered from our cDNA library suggested this variant aligned most closely with Onecut1 in the lesser devil ray (*Mobula hypostoma*). This was due to a high degree of alignment with a predicted Onecut1 spacer isoform in this other elasmobranch species. The genome assembly for this species (sMobHyp1.1) predicts that the genome sequence has the ability to produce a nearly equivalent (48 amino acid) spacer isoform, although no direct tissue specific studies have been performed and the species is endangered. However, this suggests the 48 amino acid spacer within this gene may be a broad phenomenon common to at least the batoids (skates and rays). As both the mammalian rat, and elasmobranchs have an alternative spacer exon in this gene, either the ancient common ancestor of the jawed vertebrates possessed a spacer exon which diverged into these two forms, or the evolution of spacer exons in Onecut1 results from convergent evolution. If alternative splicing of Onecut1 is a case of convergent evolution, it represents a fascinating case study on the evolution of alternative exons in general.

Methods

Preparation of Ringer's Solution

All skate Ringer's solutions were prepared as follows: 10 g Urea, 7 g NaCl, and 2 g TMAO were dissolved in 500 ml of RO water, and filter sterilized. “(Ringer’s Solution)” indicates that the

solution referred to was supplemented with this same concentration of solutes, dissolved in the standard solution. Where this label is not given, the solutions were prepared standard.

Tissue Preparation

Retinas were dissected from embryonic specimens in 1XPBS (Ringer's Solution), ensuring the preservation of the vitreous layer. The tissues were immediately fixed in 4% paraformaldehyde in 1X PBS (Ringer's Solution) for 30 minutes. The tissue was washed with PBS (Ringer's Solution) 3 times and submerged in 30% sucrose in 1x PBS (Ringer's Solution) and stored at 4°C overnight to allow for complete equilibration. The following day, sunken retinas were removed from the sucrose solution, embedded in optimal cutting temperature (OCT) compound, and rapidly frozen at -80°C. Cryosections of 20 μm thickness were obtained from the frozen tissue using a Leica cryostat. The sections were air-dried for 20 minutes and then stored at -80°C until further processing.

Antibody Staining

Frozen tissue sections were thawed in 1XPBS at room temperature prior to staining. Blocking was performed by incubating the sections in 5% serum (either goat or donkey, depending on the origin of the secondary antibody) diluted in PBT (0.1% Tween 20 for skate samples or 0.3% Triton-X in PBS for mouse tissue) for 1 hour. The sections were then incubated overnight at 4°C in the dark with primary antibodies diluted in 5% blocking solution (Normal Goat Serum) in PBT. The following day, the slides were washed three times for 15 minutes each with PBT. A second blocking step was performed by incubating the sections for 30 minutes in a 5% blocking solution in PBT. The slides were then washed three times for 5 minutes each with PBT and incubated overnight at 4°C in the dark with secondary antibodies diluted in PBT (without serum). On the third day, slides were washed again with PBT (two washes of 15 minutes each)

and a final wash with PBT containing 0.1% DAPI, protected from light. After removing the solution, the slides were mounted in Fluormount G, coverslipped, sealed with nail polish, and allowed to dry for 15 minutes to 1 hour in a fume hood. The slides were stored at 4°C before imaging.

Antibodies:

AB	Type	Catalog number
Otx2	Goat	AF1979
Onecut1	Mouse	sc-376167
Beta Gal	Mouse	DSHB 40-1a
Beta Gal	Chicken	ab9361
GFP	Chicken	ab13970
AU1	Mouse	Biolegend 901901

Microscopy Imaging

Images were collected using a Zeiss LSM 880 confocal microscope. Fluorescence channels employed included Alexa Fluor 647, Alexa Fluor 488, Cy3, and DAPI, with the specific channel used indicated in the corresponding Results sections. Laser intensity was adjusted on a case-by-case basis to maximize signal-to-noise ratio, ensuring that the signal was clearly distinguishable from background fluorescence, with care to limit bleed-through effects. Post-processing of images was performed using ImageJ (NIH). Adjustments included brightness and contrast

optimization, and color changing to enhance image clarity and ensure consistency of color scheme. Adjustments were applied equally across an image.

Embryo Selection

Embryonic little skates (*Leucoraja erinacea*) were selected for analysis based on their developmental stage, determined by visual inspection (candling). Embryos were staged according to images and described landmarks in little skates and winter skates[38,39]. At the 50 dpo stage, the embryos exhibit distinctive features such as exterior gill filaments and protruding limb buds. It should be noted that these time points are estimates and may vary slightly between individuals.

Euthanasia

To euthanize the selected embryos, they were submerged in a solution containing 1g/L Syncaine in seawater, supplemented with 2g/L sodium bicarbonate. The embryos were kept in this solution until cessation of movement and confirmed to be non-responsive and decapitated with scissors.

EdU injection

For EdU incorporation studies, 20 μL of 10 mM EdU was injected into the yolk of embryonic (~50 days post-oviposition) or hatchling little skate (*Leucoraja erinacea*). The injections were targeted to the remaining yolk on the underside of the hatchlings, ensuring proper exposure to the EdU. Following injection, the skates were allowed to recover in a seawater table for selected lengths of time before sacrifice and dissection as per the experimental design. EdU+ cells were detected using the Click-iT EdU Alexa Fluor 647 imaging kit (Invitrogen, Carlsbad, CA, USA), following the manufacturer's protocol. This method allowed for precise identification of cells that had incorporated EdU during DNA synthesis.

Anesthesia for EdU Yolk Injection

For EdU yolk injections, embryos were anesthetized by transer to a solution of 10 mg Syncaine and 20 mg sodium bicarbonate dissolved in 100 ml of seawater. The embryos were monitored for a decrease in movement to ensure effective anesthesia before proceeding with injections.

EdU Labeling Detection

For EdU labeling detection, the protocol was adapted from the immunohistochemistry (IHC) procedure previously described, as EdU detection was performed alongside antibody stainings. On the third day of the IHC protocol, after the initial 2x PBT washes, the slides were washed once with 1XPBS. A detection solution was then prepared according to the manufacturer's direction. This solution was applied to each slide at 200 μL per slide, followed by a 1-hour incubation. After incubation, the solution was removed, and the slides were washed 2 x with PBT for 15 minutes each, followed by a final wash with PBT containing 0.1% DAPI. Mounting as above under "Antibody Staining".

RNA Isolation and Quality Control

RNA was isolated with a Promega Maxwell RSC miRNA tissue kit. The RNA quality of the bulk samples was assessed using an Agilent Bioanalyzer, RIN values ranged from 8.3 to 10, indicating high RNA quality across all samples. The concentrations, as measured by the Bioanalyzer, varied from 24.4 ng/μL to 67.9 ng/μL, with corresponding total RNA amounts ranging from 610 ng to 1697.5 ng.

Paired-End Sequencing

RNA samples were sequenced on the Illumina platform (Columbia Genome Center). Paired-end sequencing was performed, generating reads with lengths 10-75 base pairs.

Sequencing Quality Control

Brief quality control metrics for each sequencing run are as follows:

- Embryonic Samples (CM003-CM005):
  - Total Sequences: 20.99-24.60 million per run
  - GC Content: 45-46%
- Hatchling Samples (CM006-CM008):
  - Total Sequences: 19.79-22.68 million per run
  - GC Content: 44-45%
- Adult Samples (CM009-CM010):
  - Total Sequences: 24.49-29.88 million per run
  - GC Content: 45%

All reads were analyzed for quality, and no sequences were flagged as poor quality across all samples.

Data Processing

The reads were aligned to the genome listed under the “Annotation” section, using the STAR aligner with two-pass mode (basic), with specific splice junction detection parameters set according to the quality of the reads and the reference genome. The resulting BAM files were then sorted and indexed for downstream analysis.

Annotation

The gene annotation file used for this project was based on the Leri_hhj_1 genome assembly (NCBI Assembly Accession: GCF_028641065.1). This annotation, which follows the GTF version 2.2 format, was provided by NCBI RefSeq with the genome build annotated on April 21, 2023. The genome assembly and the corresponding gene annotation were both sourced using the NCBI Genome Data Viewer UI. The annotation source is listed as "NCBI RefSeq GCF_028641065.1-RS_2023_04." As many genes are listed by location number in the

annotation file, a combined gene matrix was created consisting of location labeled genes (i.e. those that appear as LOC########) annotated with a long form alias, sourced in batch using NCBI's Entrez gene feature. As no short form alias was located for these genes, they were not imported into the large objects used in bioinformatic processing, but the matrix was used to identify relevant genes (Rhodopsin, Mafb). Table available on request. Gene names throughout the text are lowercase, to reflect the conventions of the datasets used to perform analysis on the skate.

Data Analysis for Bulk RNA Sequencing:

For bulk RNA sequencing analysis, gene counts were generated for each sample using the FeatureCounts tool available on the Galaxy bioinformatics platform. This process was repeated for each sequencing run. Following the feature count extraction, the counts from the two sequencing runs for each sample were averaged. The resulting averaged counts were then converted into Transcripts Per Million (TPM) to normalize the gene expression levels across samples. TPM normalization was performed by calculating the read counts per kilobase of transcript per million mapped reads for each gene, and then scaling these values such that the sum of all TPM values in a sample equals 1 million. After calculating TPM for each sample, the average TPM and standard error were computed within each experimental group (e.g., embryo, hatchling, and adult). Gene expression trajectories across developmental stages were visualized using a custom plotting script, which generated plots displaying both average TPM values and individual sample expression levels. Log10 transformation was applied to the TPM values to compress the range of expression levels and highlight subtle differences between genes.

Previously reported mouse datasets visualized for the Onecut1 genomic region were GSM2720093 (E14.1; Mus musculus; RNA-Seq; SRR5877176) and GSM2319611 (E14.5 replicate 1; Mus musculus; RNA-Seq; SRR4253086)[40,41].

cDNA Library Construction:

First-strand cDNA synthesis from the RNA samples used for the bulk RNA-seq processing was initiated by mixing 7 μL of RNA with 2 μL of a primer mix (Invitrogen, Catalog #18418012, Lot #1793155) and 1 μL of 100 mM dNTP mix (Agilent, Lot #200418-51), making up a total volume of 10 μL. The mixture was incubated at 65°C for 5 minutes, then rapidly chilled on ice. Subsequently, 4 μL of 5x Protoscript II buffer (NEB, Catalog #B0368S, Lot #10118640), 2 μL of 0.1M DTT (NEB, Catalog #B1043A, Lot #10122162), 1 μL of Protoscript II reverse transcriptase (20 U/μL) (NEB, Catalog #M0368S, Lot #10125099), 0.2 μL of RNase inhibitor (Invitrogen, Catalog #10777-019, Lot #1840422), and 2.8 μL of nuclease-free water were added to the RNA-primer mix, making the final volume 20 μL. The reaction was incubated at 42°C for 1 hour, followed by a final incubation at 65°C for 20 minutes to terminate the reaction.

Molecular Biology

To generate a little skate misexpression construct, we isolated Onecut1 cDNA from both the embryonic and adult stages of the little skate retina. Total RNA was extracted, reverse-transcribed into cDNA, and the gene was PCR-amplified. The skate Onecut1 sequence was amplified from the cDNA library using specific primers designed to flank the coding region, ensuring the preservation of the consensus ACCATG start site. The forward primer used was **GATCTCACAGAGAAAGGAC**, and the reverse primer was **ACTAGTGATCACCGAGG**. PCR amplification was carried out using Herculase polymerase, with an initial denaturation step at 95°C for 3 minutes, followed by 35 cycles of 95°C for 30 seconds, 58°C for 30 seconds, and

68°C for 75 seconds, with a final extension at 68°C for 6 minutes. The resulting PCR product was then purified and used for subsequent cloning and expression studies. The resulting PCR product was then A-tailed through incubation with Taq polymerase and dATP and cloned into the pGEM-T Easy vector. The Onecut1 insert was cut out using EcoR1 was then ligated downstream of the CAG element in a misexpression vector. For experiments involving synthetic gene fragments, full-length skate onecut1 canonical (LSOC1X1) and spacer (LSOC1X2) isoforms were obtained from Twist Bioscience, each designed with EcoRI and NotI overhangs at the 5′ and 3′ ends, respectively. Fragments were amplified using universal adapter primers and ligated into pCAG::GFP using EcoR1/Not1 and replacing GFP. Clones were confirmed by sequencing and DNA for electroporation was produced using the Qiagen Plasmid Midi Kit.

Electroporations

For both mouse and skate, electroporations followed the general procedure as used previously [42] with the following modifications and details. Skate: Retinas were harvested in Ringers L15 media and electroporation mixes were made with 40 μl 0.96M D-mannitol, 7.5 μl 10X PBS, and 10 μg each plasmid diluted in a total of 10 μl Tris-EDTA (TE) buffer. After electroporation, retinas recovered in Ringers L15 media supplemented with 10% Fetal Bovine Serum, L-glutamine, penicillin, and streptomycin and then were placed on 13mm/0.2 micron filters (10417001, Cytiva) floating on the same supplemented media. Culture was carried out at ~22 degrees for three days. Mouse: Retinas were harvested in DMEM/F12 and 5 μg of each plasmid was combined in a total volume of 50 μl 1XPBS for electroporation. A total of four retinas were electroporated for each condition and cultured at 37 degrees for two days before harvest. All electroporations used a Nepagene NEPA21 Type II Super Electroporator with 25V pulses, 50ms pulse interval, 950ms interpulse interval, for 5 total pulses.

AlphaFold Structural Modeling

AlphaFold3 models were generated using the Google AlphaFold server. We modeled:

1. Skate canonical Onecut1
2. Skate spacer Onecut1
3. Mouse canonical Onecut1
4. Truncated library-derived skate Onecut1

Sequences were sourced from NCBI Genome Data Viewer. Models included two mouse Otx2 protein sequences and the chick thrb-CRM1 sequence (40 bp upstream regulatory element: ACACGCTGAAAATCCTAAAATCAATAATCCTGTTTTTCAGC). The reverse complement was also provided to model DNA as a double helix. Complexes were visualized in PyMOL to examine DNA binding domains.

TBLASTN Analysis

We used NCBI BLAST+ v2.16.0 to perform TBLASTN searches comparing elephant shark protein sequences to pseudogenized regions of the little skate genome. Commands included:

tblastn -query [elephant_shark_protein.fasta] -subject [little_skate_region.fasta] -out [report.txt] -outfmt 0

The -outfmt 0 option produced traditional BLAST reports, including tables of sequences producing significant alignments (bit scores, e-values) and formatted alignments showing residue matches and coordinate positions. These reports were used to evaluate homology.

Acknowledgements: Funding for this project was provided to M.E. by NSF CAREER Award 1453044, PSC-CUNY award ENHC-54-105, and the MBL Whitman Fellows Program with support from the Hartline MacNichol Research Award and the Fries Trust Research Awards, L.&A Colwin Summer Research Fellowship Fund. D.M. was supported by a Graduate Research Training Initiative for Student Enhancement grant from the National Institute of General Medical Sciences to The City College of New York (5T32GM136499-05). We thank Laura Alexander for assistance with RNA isolation, Miruna Ghinia-Tegla for technical guidance on bulk-RNA sequencing, Angelina Grebe for consultation on the potential implications of this discovery at the structural level, Michael Palmer for skate tissue culture assistance, Ken Hastings for marine electroporation guidance, and Sruti Patoori for preliminary investigation of the skate retina. We thank the MBL staff of the Marine Resource Center including Nolan Gibbons, Brian McGonagle, Lisa Abbo, and Dave Remsen for assistance with the use and care of specimens. We thank all members of the Emerson Lab for support throughout the project.

FIGURE LEGENDS

FIGURE 1 Thymidine birthdating analysis of embryonic little skate retina and electroporation of broad and specific transcriptional reporters.
(A) Embryonic (50 dpo) retina pulse labeled with EdU for 4 hours, stained for EdU--magenta (Alexa Fluor 647), otx2--yellow (Alexa Fluor 488), and phospho histone H3 (PHH3)--white (Cy3). Solid white box indicates representative otx2+/EdU+ cell. Dashed white box indicates representative EdU-/PHH3+ dividing nucleus. (B) Magnified image of otx2+/EdU+ nucleus (B') otx2 signal alone. (C) Zoom in of EdU-/PHH3+ nucleus representative, with both channels (EdU, PHH3) visualized. (C') C image with PHH3 channel removed. (D) 8 hour labeled 50 dpo retina. Dashed box indicates representative EdU+/PHH3+ nucleus. (E) Magnified image of PHH3+/EdU+ nucleus with both channels (EdU, PHH3) present. (E') E image with PHH3 channel removed. (F) Bar graph showing percent of dividing nuclei (PHH3+) with interior EdU at time of retinal fixation, by incubation length. $p<0.001$ by Welch's t-test. (G,H) ~50 dpo little skate retina electroporated with CAG::GFP and CAG::mCherry and visualized in wholemount for mCherry (G) and GFP (H). (I-K) Sections of retinas electroporated as in G,H with signals noted on panel. (L,M) ~50 dpo little skate retina electroporated with CAG::mCherry and ThrbCRM1::GFP and visualized in wholemount for mCherry (L) and GFP (M).

FIGURE 2 Developmental gene expression profiles of photoreceptor expressed genes and correlations to cone and rod presence.

(A) Developmental gene trajectory of eight selected photoreceptor developmental markers [mafb, otx5 (crx), mafaa, nr2e3, rorb, thrb, onecut1, rxrga, and otx2b], as well as control purine salvage enzyme gene hprt1. Blue indicate predominantly rod associated genes and red indicates predominantly cone associated genes. (B) Mature phototransduction gene trajectories. (C) (Top) Cone associated genes from A visualized alone with Otx2b included (Bottom) Rod associated genes. Otx5, or crx is necessary for both cone and rod specification in other vertebrates, and is included with the rod program due to its known collaboration with Maf to drive nr2e3. By TPM, otx5 exhibits the highest general expression of photoreceptor related developmental genes. (D) Table of cone phototransduction gene conservation among the Chondrichthyes lineage. Little skate highlighted in brown. Phylogenetic tree indicates clade divergence times (based on Marletaz et. al., 2023). "Pseudo" indicates the standard reference sequence annotates the gene as a pseudogene (as per NCBI's Genome Data Viewer).+ indicates the gene was annotated in a conserved location (relative to elephant shark). n.f indicates the gene was not found in the conserved location.

FIGURE 3 Alternative splicing of Onecut1 results in two isoforms with stage-specific expression ratios

(A)Schematic of the little skate onecut1 genetic locus. Black box indicates exon 1; yellow box is exon 2; small blue box is the spacer exon; magenta box is exon 3. Observed alternative splicing indicates the presence of two Onecut1 isoforms: canonical OC1 and the OC1 spacer variant. The third splice event represents the truncated spacer variant that led to the identification of the complete OC1 spacer variant. (B) OC1 locus with annotated features. Truncation query sequence is labeled in exon 1, spacer query sequence is labeled at the 3' end of exon 2. Region truncated from the canonical OC1 spans the first 2 exons ("Truncated Region"). Spacer isoform identifier "GGA" labeled at the 5' end of the spacer exon. Canonical isoform identifier (CGT) labeled at the 5' end of exon 3. DBDs labeled in their rough relative location within the locus. Distances roughly approximate relative genomic distances between annotated features. (C) (Top) Representative alignment of canonical reference sequence (standard reference's annotated onecut1) with mapped reads containing spacer query (black, bold). (Middle) Magenta sequence shows canonical continuation from the end of exon 2. Bold, underlined "CGT" is 3 bp canonical isoform identifier. Blue sequence shows spacer exon continuing from exon 2, in a majority of reads in the embryo. Bold, underlined "GGA" indicates 3 bp spacer isoform identifier. (Bottom) Alignment of spacer isoform sequence (region of recovered onecut1 from cDNA library). Blue sequence indicates beginning of spacer exon, bold underlined "GGA" the spacer isoform identifying sequence. (D) Bar plot showing the ratio of isoforms across 3 stages of development. Spacer isoform represented in blue, canonical in magenta. Read counts-Embryo: 75 reads, Hatchling: 25 reads, Adult: 9 reads. Chi squared = 21.4, 2 df. $p<0.0001$.

FIGURE 4 Novel Onecut1 Spacer Isoform Validated as Functional Protein, Activates the thrbCRM1 Reporter Element

(A) Alphafold3 models predicting the binding properties of one variable molecule of OC1 (mouse, skate canonical, skate spacer isoform), two molecules of OTX2 and the thrbCRM1 element double helix. All DBDs, OC1 linker, spacer shown, as well as thrbCRM1. OC1 CUT (blue), HD (red), spacer element (yellow), and canonical linker (green) labeled. OTX2 HD

labeled in orange. (B-E) P0 mouse retinas electroporated ex vivo with ThrbCRM1::GFP, pCAG::Bgal, and a pCAG construct that drives the expression of the Onecut1 transcript denoted on the left of each row. After 2 days, retinas were harvested and processed for confocal microscopy to visualize nuclei (DAPI in blue), GFP reporter (yellow), Bgal (magenta) and OC1 protein (white) which is detected in unelectroporated mouse horizontal cells in all retinas and any electroporated cell that expresses a OC1 protein that is recognized by the antibody. Visualized channels are shown above each row. (B) pCAG::NULL negative control: pCAG expression vector with no encoded protein sequence (C) pCAG :: mouse onecut1. (C) pCAG::LSOC1X1 (D) pCAG::LSOC1X2. Scale bars are all 50um.

SUPPLEMENTAL FIGURE LEGENDS:

Supplemental Figure S1. PHH3 and EdU labeling in early and late time points.

(A) Table showing counts of PHH3+ cells and EdU+ cells in the 4-hour and 8-hour post-injection groups. **(B)** Representative images from the 2-hour and 40-hour EdU groups. Arrowheads mark PHH3+ cells. Top left: 2-hour group showing PHH3+ (white) cells and EdU (magenta); top right: same field with PHH3 channel off showing absence of EdU signal at arrowhead positions, indicating no EdU incorporation in PHH3+ cells at this early time point. Bottom left: 40-hour group with PHH3 staining (magenta) and EdU (white); Bottom right: same field with PHH3 channel turned off and EdU signal (white) visible, demonstrating that all PHH3+ cells are also EdU+. **(c)** DAPI+ overview images of representative sections from the 2-, 4-, 8-, and 40-hour EdU groups, corresponding to those shown in Figure 1 and panel (b), to visualize the relative abundance of EdU-labeled nuclei (magenta) across time points.

Supplemental Figure 2: Comparative expression and genomic context of cone phototransduction genes absent in the skate genome.

(A) TBLASTN alignments of elephant shark protein-coding sequences to corresponding *Leucoraja erinacea* genomic regions for pde6c, arr3 and gnat2. Nonsense mutations highlighted in otherwise highly conserved regions (pde6c: E = 3e-28, arr3: E = 3e-09, gnat2: E = 8e-18).

(B) Genome tracks from NCBI Genome Data Viewer illustrating the genomic regions surrounding flanking genes of cone phototransduction genes present in the elephant shark but absent in skate (arr3, gnat2, pde6c). The immediate flanking genes were conserved across *Leucoraja erinacea, Scyliorhinus canicula, Mobula hypostoma, and Callorhinchus milii,* indicating preserved local synteny despite loss or degradation of the phototransduction genes themselves. **(C)** Table showing the average transcripts per million (TPM) values for all genes plotted in Figure 2 across developmental stages.

Supplemental Figure S3: Analysis of *Onecut1* splice isoform usage and spacer region conservation across development and species.

(A) Table of the number and frequency of Onecut1 spacer and canonical isoform reads at three developmental stages in little skate. **(B)** IGV screenshots comparing RNA-seq coverage and splice junctions across the Onecut1 locus in little skate and mouse embryonic retina. The little

skate embryo (~50 dpo) shows abundant inclusion of a spacer exon (arrowhead), supported by junction-spanning reads. In contrast, wild-type C57BL/6N mouse retina at E14.5 (Brooks et al., 2019; panel B′) and C57BL/6 mouse retina at E14.5 (Aldiri et al., 2017; panel B″) display canonical splicing of onecut1 exons 1 and 2 with minimal inclusion of the analogous spacer region. Both mouse datasets show low-level read coverage in a region encoding codons analogous to the rat liver onecut1 spacer exon, but expression in this region is less than that of the embryonic skate spacer exon, and its functional significance is unclear. **(C)** Alignment of spacer region protein sequences from Onecut1 transcripts across four myliobatiform species (*Mobula hypostoma*, *Hypanus sabinus*, *Hemitrygon akajei*, *Narcine bancroftii*) compared to *Leucoraja erinacea* (little skate). Sequences were obtained from NCBI standard reference genomes: *Mobula hypostoma*: sMobHyp1.1, *Hypanus sabinus*: sHypSab1.hap1, *Hemitrygon akajei*: sHemAka1.3, *Narcine bancroftii*: sNarBan1.hap1. Blue indicates conservative amino acid substitutions relative to skate; red indicates non-conservative substitutions. **(D)** Alignment of bulk RNA-seq reads containing the truncation query sequence (5′-ACAAGGAGAT-3′) to the Onecut1 cDNA library-derived sequence and the reference genomic sequence. All query-matching reads aligned to the canonical reference continuation (green), with occasional single nucleotide variants (grey). No reads matched the cDNA library-derived continuation (red), suggesting it is a technical artifact.

Supplemental Figure S4: Structural modeling and functional assay of the truncated skate onecut1 isoform.

(A) Electroporation assay testing activation of the ThrbCRM1 reporter by different Onecut1 constructs. Retinal sections show electroporation of control (pCAG::null), CAG::mouse Onecut1, or CAG::truncated skate Onecut1 along with ThrbCRM1::AU1 reporter and CAG::GFP for electroporation tracking. In the control (top row), no AU1 signal (yellow) is detected in GFP-positive regions (white) and Onecut1 antibody staining (magenta) labels endogenous Onecut1 expression in horizontal cells. CAG::mouse Onecut1 induces AU1 reporter activity (arrowheads, bottom row), consistent with activation of ThrbCRM1 and presence of ectopic Onecut1 protein signal. The truncated skate Onecut1 was not observed to drive ThrbCRM1::AU1 reporter. **(B)** PyMOL rendering of the AlphaFold-predicted structure of the truncated skate Onecut1 isoform, derived from cDNA, bound to the ThrbCRM1 element along with two molecules of mouse Otx2. The DNA binding domains are conserved and bind globally in a manner similar to the full-length skate Onecut1 spacer isoform (LSOC1X2).

References

(1) Hahn, J.; Monavarfeshani, A.; Qiao, M.; Kao, A. H.; Kölsch, Y.; Kumar, A.; Kunze, V. P.; Rasys, A. M.; Richardson, R.; Wekselblatt, J. B.; Baier, H.; Lucas, R. J.; Li, W.; Meister, M.; Trachtenberg, J. T.; Yan, W.; Peng, Y.-R.; Sanes, J. R.; Shekhar, K. Evolution of Neuronal Cell Classes and Types in the Vertebrate Retina. *Nature* **2023**, *624* (7991), 415–424. https://doi.org/10.1038/s41586-023-06638-9.

(2) Mahabadi, N.; Al Khalili, Y. Neuroanatomy, Retina. In *StatPearls*; StatPearls Publishing: Treasure Island (FL), 2025.

(3) Lamb, T. D. Evolution of Phototransduction, Vertebrate Photoreceptors and Retina. *Prog. Retin. Eye Res.* **2013**, *36*, 52–119. https://doi.org/10.1016/j.preteyeres.2013.06.001.

(4) Bowmaker, J. K. Evolution of Colour Vision in Vertebrates. *Eye Lond. Engl.* **1998**, *12 (Pt 3b)*, 541–547. https://doi.org/10.1038/eye.1998.143.

(5) Dowling, J. E.; Ripps, H. On the Duplex Nature of the Skate Retina. *J. Exp. Zool. Suppl. Publ. Auspices Am. Soc. Zool. Div. Comp. Physiol. Biochem.* **1990**, *5*, 55–65. https://doi.org/10.1002/jez.1402560509.

(6) Warrant, E. J. Photoreceptor Evolution: Ancient "cones" Turn out to Be Rods. *Curr. Biol. CB* **2015**, *25* (4), R148-151. https://doi.org/10.1016/j.cub.2015.01.005.

(7) Lisney, T. J.; Theiss, S. M.; Collin, S. P.; Hart, N. S. Vision in Elasmobranchs and Their Relatives: 21st Century Advances. *J. Fish Biol.* **2012**, *80* (5), 2024–2054. https://doi.org/10.1111/j.1095-8649.2012.03253.x.

(8) Hart, N. S. Vision in Sharks and Rays: Opsin Diversity and Colour Vision. *Semin. Cell Dev. Biol.* **2020**, *106*, 12–19. https://doi.org/10.1016/j.semcdb.2020.03.012.

(9) Magaña-Hernández, L.; Wagh, A. S.; Fathi, J. G.; Robles, J. E.; Rubio, B.; Yusuf, Y.; Rose, E. E.; Brown, D. E.; Perry, P. E.; Hamada, E.; Anastassov, I. A. Ultrastructural Characteristics and Synaptic Connectivity of Photoreceptors in the Simplex Retina of Little Skate (Leucoraja Erinacea). *eNeuro* **2023**, *10* (10), ENEURO.0226-23.2023. https://doi.org/10.1523/ENEURO.0226-23.2023.

(10) Young, R. W. Cell Differentiation in the Retina of the Mouse. *Anat. Rec.* **1985**, *212* (2), 199–205. https://doi.org/10.1002/ar.1092120215.

(11) Emerson, M. M.; Surzenko, N.; Goetz, J.; Trimarchi, J. M.; Cepko, C. Otx2 and Onecut1 Promote the Fates of Cone Photoreceptors and Horizontal Cells and Repress Rod Photoreceptors. *Dev. Cell* **2013**, *26* (1), 59–72.

(12) Wu, F.; Sapkota, D.; Li, R.; Mu, X. Onecut 1 and Onecut 2 Are Potential Regulators of Mouse Retinal Development. *J. Comp. Neurol.* **2012**, *520* (5), 952–969. https://doi.org/10.1002/cne.22741.

(13) Corbo, J. C.; Levine, M.; Zeller, R. W. Characterization of a Notochord-Specific Enhancer from the Brachyury Promoter Region of the Ascidian, Ciona Intestinalis. *Dev. Camb. Engl.* **1997**, *124* (3), 589–602. https://doi.org/10.1242/dev.124.3.589.

(14) Niwa, H.; Yamamura, K.; Miyazaki, J. Efficient Selection for High-Expression Transfectants with a Novel Eukaryotic Vector. *Gene* **1991**, *108* (2), 193–199.

(15) Haider, N. B.; Jacobson, S. G.; Cideciyan, A. V.; Swiderski, R.; Streb, L. M.; Searby, C.; Beck, G.; Hockey, R.; Hanna, D. B.; Gorman, S.; Duhl, D.; Carmi, R.; Bennett, J.; Weleber, R. G.; Fishman, G. A.; Wright, A. F.; Stone, E. M.; Sheffield, V. C. Mutation of a Nuclear Receptor Gene, NR2E3, Causes Enhanced S Cone Syndrome, a Disorder of Retinal Cell Fate. *Nat. Genet.* **2000**, *24* (2), 127–131. https://doi.org/10.1038/72777.

(16) Chen, J.; Rattner, A.; Nathans, J. The Rod Photoreceptor-Specific Nuclear Receptor Nr2e3 Represses Transcription of Multiple Cone-Specific Genes. *J. Neurosci. Off. J. Soc. Neurosci.* **2005**, *25* (1), 118–129. https://doi.org/10.1523/JNEUROSCI.3571-04.2005.
(17) Corbo, J. C.; Cepko, C. L. A Hybrid Photoreceptor Expressing Both Rod and Cone Genes in a Mouse Model of Enhanced S-Cone Syndrome. *PLoS Genet.* **2005**, *1* (2), e11. https://doi.org/10.1371/journal.pgen.0010011.
(18) Jean-Charles, N.; Buenaventura, D. F.; Emerson, M. M. Identification and Characterization of Early Photoreceptor Cis-Regulatory Elements and Their Relation to Onecut1. *Neural Develop.* **2018**, *13* (1), 26. https://doi.org/10.1186/s13064-018-0121-x.
(19) Ogino, H.; Yasuda, K. Induction of Lens Differentiation by Activation of a bZIP Transcription Factor, L-Maf. *Science* **1998**, *280* (5360), 115–118.
(20) Ochi, H.; Sakagami, K.; Ishii, A.; Morita, N.; Nishiuchi, M.; Ogino, H.; Yasuda, K. Temporal Expression of L-Maf and RaxL in Developing Chicken Retina Are Arranged into Mosaic Pattern. *Gene Expr. Patterns GEP* **2004**, *4* (5), 489–494. https://doi.org/10.1016/j.modgep.2004.03.005.
(21) Mears, A. J.; Kondo, M.; Swain, P. K.; Takada, Y.; Bush, R. A.; Saunders, T. L.; Sieving, P. A.; Swaroop, A. Nrl Is Required for Rod Photoreceptor Development. *Nat. Genet.* **2001**, *29* (4), 447–452. https://doi.org/10.1038/ng774.
(22) Marlétaz, F.; de la Calle-Mustienes, E.; Acemel, R. D.; Paliou, C.; Naranjo, S.; Martínez-García, P. M.; Cases, I.; Sleight, V. A.; Hirschberger, C.; Marcet-Houben, M.; Navon, D.; Andrescavage, A.; Skvortsova, K.; Duckett, P. E.; González-Rajal, Á.; Bogdanovic, O.; Gibcus, J. H.; Yang, L.; Gallardo-Fuentes, L.; Sospedra, I.; Lopez-Rios, J.; Darbellay, F.; Visel, A.; Dekker, J.; Shubin, N.; Gabaldón, T.; Nakamura, T.; Tena, J. J.; Lupiáñez, D. G.; Rokhsar, D. S.; Gómez-Skarmeta, J. L. The Little Skate Genome and the Evolutionary Emergence of Wing-like Fins. *Nature* **2023**, *616* (7957), 495–503. https://doi.org/10.1038/s41586-023-05868-1.
(23) Bozzanao, A.; Murgia, R.; Vallerga, S.; Hirano, J.; Archer, S. The Photoreceptor System in the Retinae of Two Dogfishes, Scyliorhinus Canicula and Galeus Melastomus: Possible Relationship with Depth Distribution and Predatory Lifestyle. *J. Fish Biol.* **2001**, *59* (5), 1258–1278. https://doi.org/10.1111/j.1095-8649.2001.tb00190.x.
(24) Hart, N. S.; Lamb, T. D.; Patel, H. R.; Chuah, A.; Natoli, R. C.; Hudson, N. J.; Cutmore, S. C.; Davies, W. I. L.; Collin, S. P.; Hunt, D. M. Visual Opsin Diversity in Sharks and Rays. *Mol. Biol. Evol.* **2020**, *37* (3), 811–827. https://doi.org/10.1093/molbev/msz269.
(25) Lannoy, V. J.; Bürglin, T. R.; Rousseau, G. G.; Lemaigre, F. P. Isoforms of Hepatocyte Nuclear Factor-6 Differ in DNA-Binding Properties, Contain a Bifunctional Homeodomain, and Define the New ONECUT Class of Homeodomain Proteins. *J. Biol. Chem.* **1998**, *273* (22), 13552–13562. https://doi.org/10.1074/jbc.273.22.13552.
(26) van Leeuwen, H. C.; Strating, M. J.; Rensen, M.; de Laat, W.; van der Vliet, P. C. Linker Length and Composition Influence the Flexibility of Oct-1 DNA Binding. *EMBO J.* **1997**, *16* (8), 2043–2053. https://doi.org/10.1093/emboj/16.8.2043.
(27) Lonfat, N.; Wang, S.; Lee, C.; Garcia, M.; Choi, J.; Park, P. J.; Cepko, C. Cis-Regulatory Dissection of Cone Development Reveals a Broad Role for Otx2 and Oc Transcription Factors. *Dev. Camb. Engl.* **2021**, *148* (9), dev198549. https://doi.org/10.1242/dev.198549.
(28) Abramson, J.; Adler, J.; Dunger, J.; Evans, R.; Green, T.; Pritzel, A.; Ronneberger, O.; Willmore, L.; Ballard, A. J.; Bambrick, J.; Bodenstein, S. W.; Evans, D. A.; Hung, C.-C.; O'Neill, M.; Reiman, D.; Tunyasuvunakool, K.; Wu, Z.; Žemgulytė, A.; Arvaniti, E.; Beattie, C.; Bertolli, O.; Bridgland, A.; Cherepanov, A.; Congreve, M.; Cowen-Rivers, A. I.; Cowie, A.;

Figurnov, M.; Fuchs, F. B.; Gladman, H.; Jain, R.; Khan, Y. A.; Low, C. M. R.; Perlin, K.; Potapenko, A.; Savy, P.; Singh, S.; Stecula, A.; Thillaisundaram, A.; Tong, C.; Yakneen, S.; Zhong, E. D.; Zielinski, M.; Žídek, A.; Bapst, V.; Kohli, P.; Jaderberg, M.; Hassabis, D.; Jumper, J. M. Accurate Structure Prediction of Biomolecular Interactions with AlphaFold 3. *Nature* **2024**, *630* (8016), 493–500. https://doi.org/10.1038/s41586-024-07487-w.
(29) Matsuda, T.; Cepko, C. L. Electroporation and RNA Interference in the Rodent Retina in Vivo and in Vitro. *Proc. Natl. Acad. Sci. U. S. A.* **2004**, *101* (1), 16–22. https://doi.org/10.1073/pnas.2235688100.
(30) Cepko, C. Intrinsically Different Retinal Progenitor Cells Produce Specific Types of Progeny. *Nat. Rev. Neurosci.* **2014**, *15* (9), 615–627. https://doi.org/10.1038/nrn3767.
(31) Hafler, B. P.; Surzenko, N.; Beier, K. T.; Punzo, C.; Trimarchi, J. M.; Kong, J. H.; Cepko, C. L. Transcription Factor Olig2 Defines Subpopulations of Retinal Progenitor Cells Biased toward Specific Cell Fates. *Proc. Natl. Acad. Sci. U. S. A.* **2012**, *109* (20), 7882–7887. https://doi.org/10.1073/pnas.1203138109.
(32) Wang, S.; Cepko, C. L. Photoreceptor Fate Determination in the Vertebrate Retina. *Invest. Ophthalmol. Vis. Sci.* **2016**, *57* (5), ORSFe1-6. https://doi.org/10.1167/iovs.15-17672.
(33) Oh, E. C. T.; Khan, N.; Novelli, E.; Khanna, H.; Strettoi, E.; Swaroop, A. Transformation of Cone Precursors to Functional Rod Photoreceptors by bZIP Transcription Factor NRL. *Proc. Natl. Acad. Sci. U. S. A.* **2007**, *104* (5), 1679–1684. https://doi.org/10.1073/pnas.0605934104.
(34) Sapkota, D.; Chintala, H.; Wu, F.; Fliesler, S. J.; Hu, Z.; Mu, X. Onecut1 and Onecut2 Redundantly Regulate Early Retinal Cell Fates during Development. *Proc. Natl. Acad. Sci. U. S. A.* **2014**, *111* (39), E4086-4095. https://doi.org/10.1073/pnas.1405354111.
(35) Yamamoto, K.; Matsuoka, T.; Kawashima, S.; Takebe, S.; Kubo, F.; Miyatsuka, T.; Kaneto, H.; Shimomura, I. A Novel Function of Onecut1 Protein as a Negative Regulator of MafA Gene Expression. *J. Biol. Chem.* **2013**, *288* (30), 21648–21658. https://doi.org/10.1074/jbc.M113.481424.
(36) Pierreux, C. E.; Stafford, J.; Demonte, D.; Scott, D. K.; Vandenhaute, J.; O'Brien, R. M.; Granner, D. K.; Rousseau, G. G.; Lemaigre, F. P. Antiglucocorticoid Activity of Hepatocyte Nuclear Factor-6. *Proc. Natl. Acad. Sci. U. S. A.* **1999**, *96* (16), 8961–8966. https://doi.org/10.1073/pnas.96.16.8961.
(37) Vidal-Vázquez, N.; Hernández-Núñez, I.; Carballo-Pacoret, P.; Salisbury, S.; Villamayor, P. R.; Hervas-Sotomayor, F.; Yuan, X.; Lamanna, F.; Schneider, C.; Schmidt, J.; Mazan, S.; Kaessmann, H.; Adrio, F.; Robledo, D.; Barreiro-Iglesias, A.; Candal, E. A Single-Nucleus RNA Sequencing Atlas of the Postnatal Retina of the Shark Scyliorhinus Canicula. *Sci. Data* **2025**, *12* (1), 228. https://doi.org/10.1038/s41597-025-04547-2.
(38) Maxwell, E. E.; Fröbisch, N. B.; Heppleston, A. C. Variability and Conservation in Late Chondrichthyan Development: Ontogeny of the Winter Skate (Leucoraja Ocellata). *Anat. Rec. Hoboken NJ 2007* **2008**, *291* (9), 1079–1087. https://doi.org/10.1002/ar.20719.
(39) Gillis, J. A.; Bennett, S.; Criswell, K. E.; Rees, J.; Sleight, V. A.; Hirschberger, C.; Calzarette, D.; Kerr, S.; Dasen, J. Big Insight from the Little Skate: Leucoraja Erinacea as a Developmental Model System. *Curr. Top. Dev. Biol.* **2022**, *147*, 595–630. https://doi.org/10.1016/bs.ctdb.2021.12.016.
(40) Aldiri, I.; Xu, B.; Wang, L.; Chen, X.; Hiler, D.; Griffiths, L.; Valentine, M.; Shirinifard, A.; Thiagarajan, S.; Sablauer, A.; Barabas, M.-E.; Zhang, J.; Johnson, D.; Frase, S.; Zhou, X.; Easton, J.; Zhang, J.; Mardis, E. R.; Wilson, R. K.; Downing, J. R.; Dyer, M. A.; St. Jude Children's Research Hospital—Washington University Pediatric Cancer Genome Project. The

Dynamic Epigenetic Landscape of the Retina During Development, Reprogramming, and Tumorigenesis. *Neuron* **2017**, *94* (3), 550-568.e10. https://doi.org/10.1016/j.neuron.2017.04.022.
(41) Brooks, M. J.; Chen, H. Y.; Kelley, R. A.; Mondal, A. K.; Nagashima, K.; De Val, N.; Li, T.; Chaitankar, V.; Swaroop, A. Improved Retinal Organoid Differentiation by Modulating Signaling Pathways Revealed by Comparative Transcriptome Analyses with Development In Vivo. *Stem Cell Rep.* **2019**, *13* (5), 891–905. https://doi.org/10.1016/j.stemcr.2019.09.009.
(42) Emerson, M. M.; Cepko, C. L. Identification of a Retina-Specific Otx2 Enhancer Element Active in Immature Developing Photoreceptors. *Dev. Biol.* **2011**, *360* (1), 241–255. https://doi.org/10.1016/j.ydbio.2011.09.012.

Figure 1

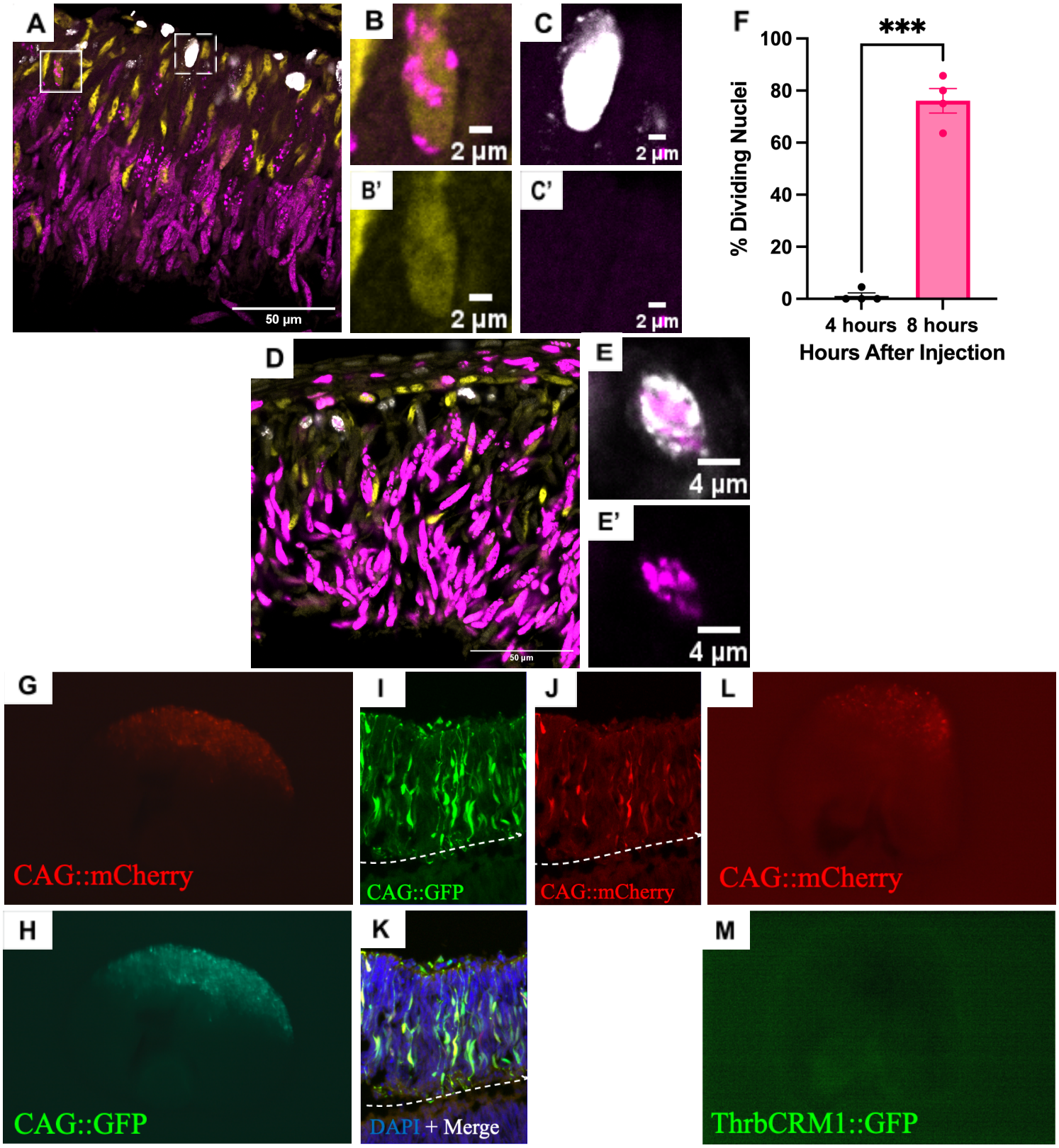
A
50 µm
B
2 µm
B'
2 µm
C
2 µm
C'
2 µm
D
50 µm
E
4 µm
E'
4 µm
F
***
% Dividing Nuclei
100
80
60
40
20
0
4 hours
8 hours
Hours After Injection
G
CAG::mCherry
I
CAG::GFP
J
CAG::mCherry
L
CAG::mCherry
H
CAG::GFP
K
DAPI + Merge
M
ThrbCRM1::GFP

FIGURE 2

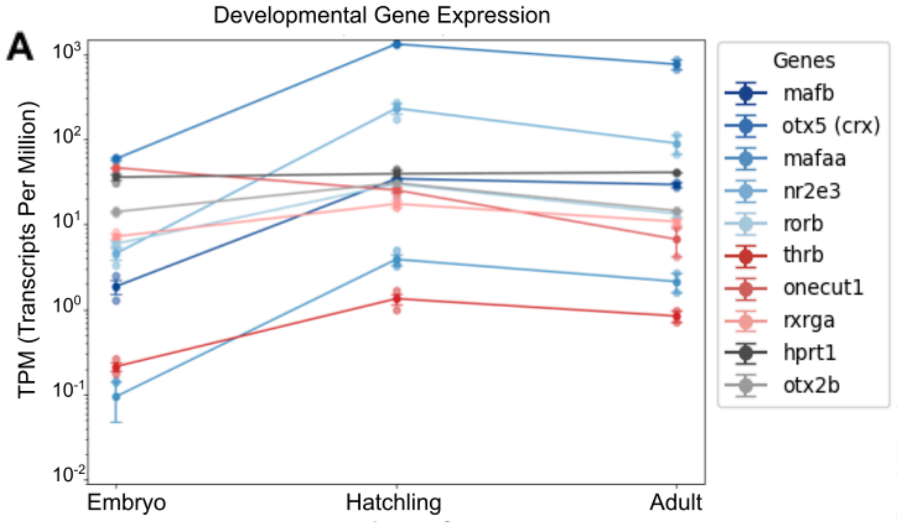

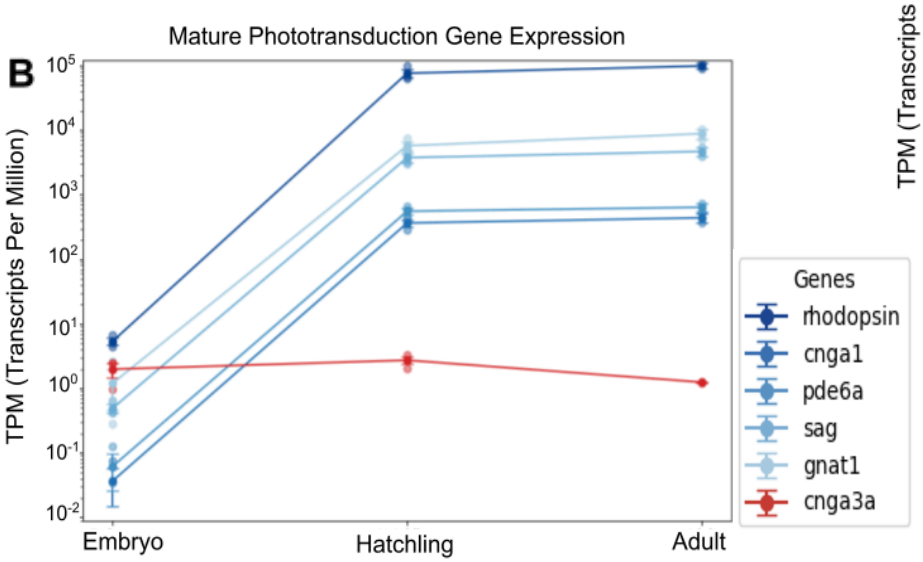

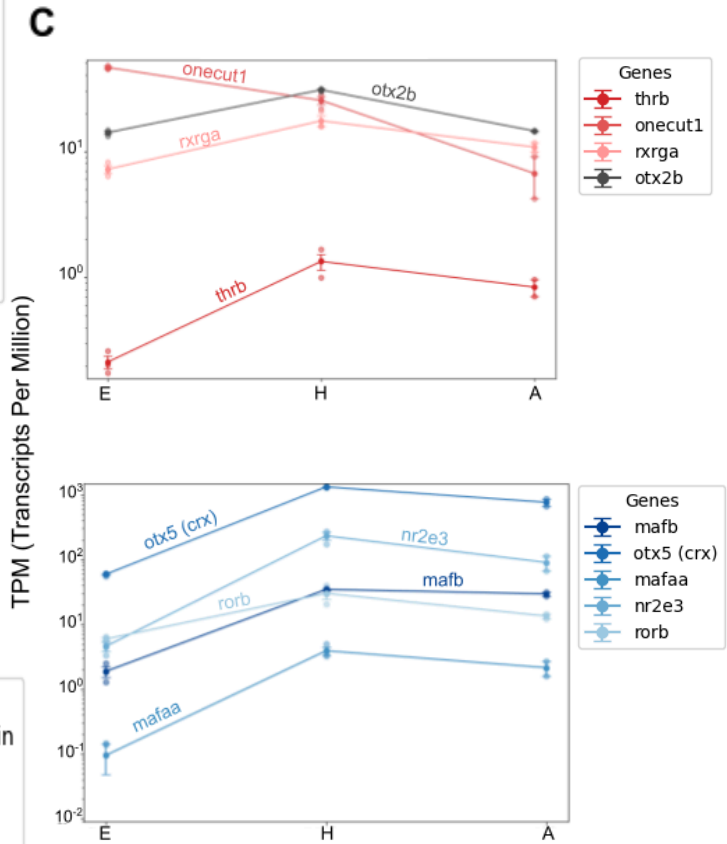

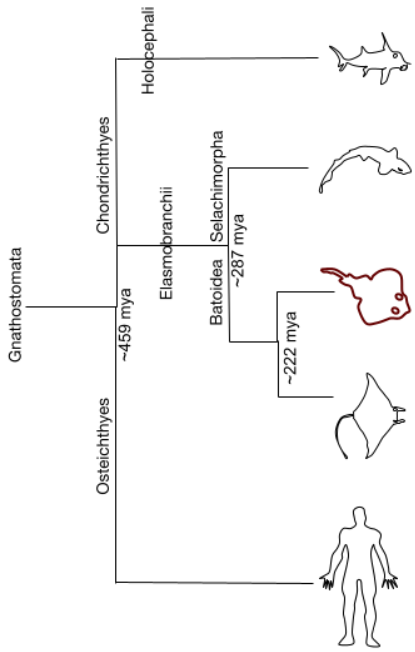

Cones	gnat2	pde6c	arr3	rh2	lws1	lws2
Red, green, blue	+	+	+	+	+	+
limited/ none reported*	pseudo	+	n.f.	+	n.f.	n.f.
none reported	n.f.	n.f.	n.f.	n.f.	n.f.	n.f.
long wave sensitive, short wave sensitive	+	+	n.f.	+	n.f.	+

FIGURE 3

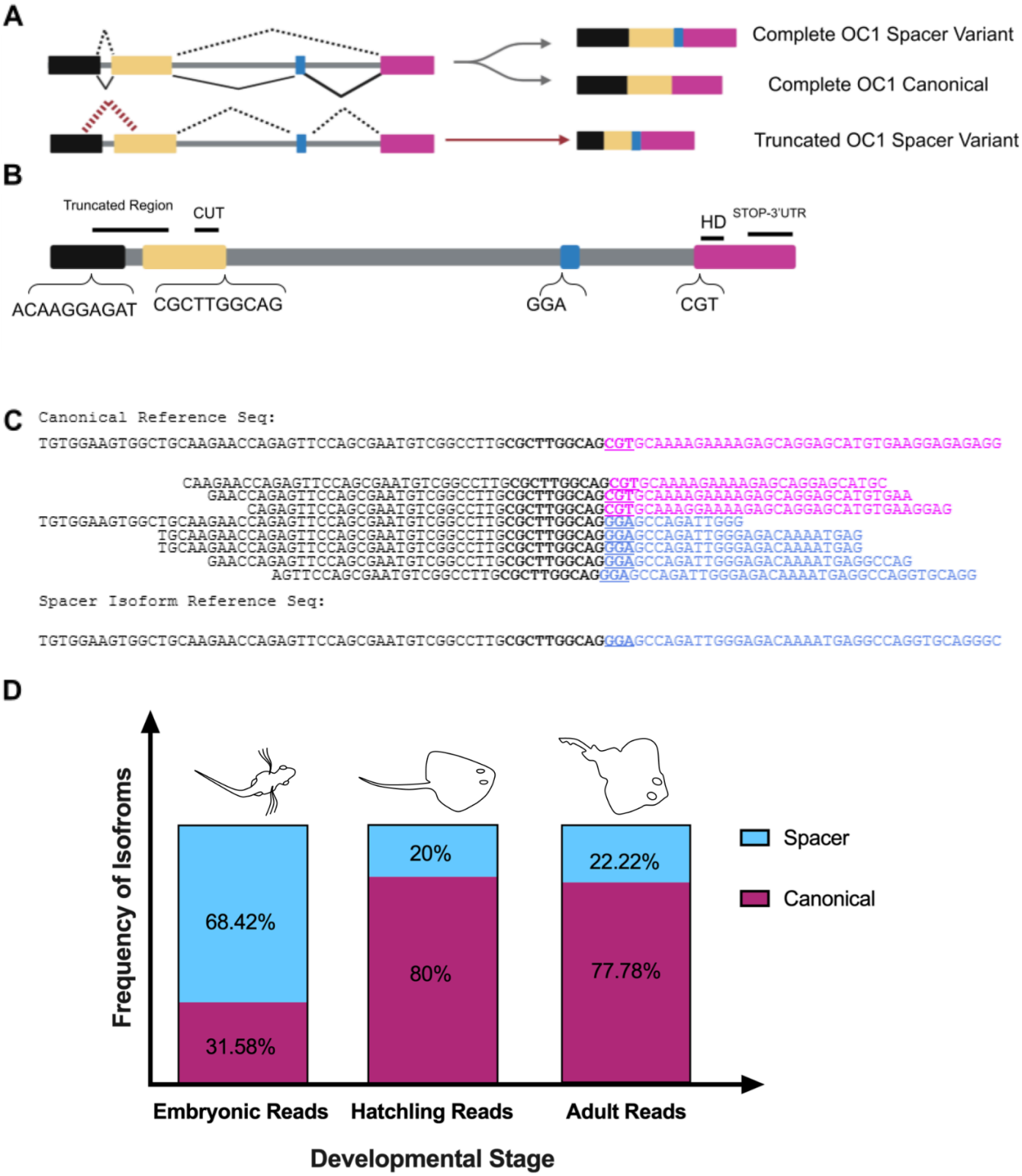
A
Complete OC1 Spacer Variant
Complete OC1 Canonical
Truncated OC1 Spacer Variant
B
Truncated Region
CUT
HD
STOP-3'UTR
ACAAGGAGAT
CGCTTGGCAG
GGA
CGT
C
Canonical Reference Seq:
TGTGGAAGTGGCTGCAAGAACCAGAGTTCCAGCGAATGTCGGCCTTGCGCTTGGCAGCGTGCAAAAGAAAAGAGCAGGAGCATGTGAAGGAGAGAGG
CAAGAACCAGAGTTCCAGCGAATGTCGGCCTTGCGCTTGGCAGCGTGCAAAAGAAAAGAGCAGGAGCATGC
GAACCAGAGTTCCAGCGAATGTCGGCCTTGCGCTTGGCAGCGTGCAAAAGAAAAGAGCAGGAGCATGTGAA
CAGAGTTCCAGCGAATGTCGGCCTTGCGCTTGGCAGCGTGCAAAGGAAAAGAGCAGGAGCATGTGAAGGAG
TGTGGAAGTGGCTGCAAGAACCAGAGTTCCAGCGAATGTCGGCCTTGCGCTTGGCAGGGAGCCAGATTGGG
TGCAAGAACCAGAGTTCCAGCGAATGTCGGCCTTGCGCTTGGCAGGGAGCCAGATTGGGAGACAAAATGAG
TGCAAGAACCAGAGTTCCAGCGAATGTCGGCCTTGCGCTTGGCAGGGAGCCAGATTGGGAGACAAAATGAG
GAACCAGAGTTCCAGCGAATGTCGGCCTTGCGCTTGGCAGGGAGCCAGATTGGGAGACAAAATGAGGCCAG
AGTTCCAGCGAATGTCGGCCTTGCGCTTGGCAGGGAGCCAGATTGGGAGACAAAATGAGGCCAGGTGCAGG
Spacer Isoform Reference Seq:
TGTGGAAGTGGCTGCAAGAACCAGAGTTCCAGCGAATGTCGGCCTTGCGCTTGGCAGGGAGCCAGATTGGGAGACAAAATGAGGCCAGGTGCAGGGC
D
Frequency of Isofroms
68.42%
31.58%
20%
80%
22.22%
77.78%
Spacer
Canonical
Embryonic Reads
Hatchling Reads
Adult Reads
Developmental Stage

FIGURE 4

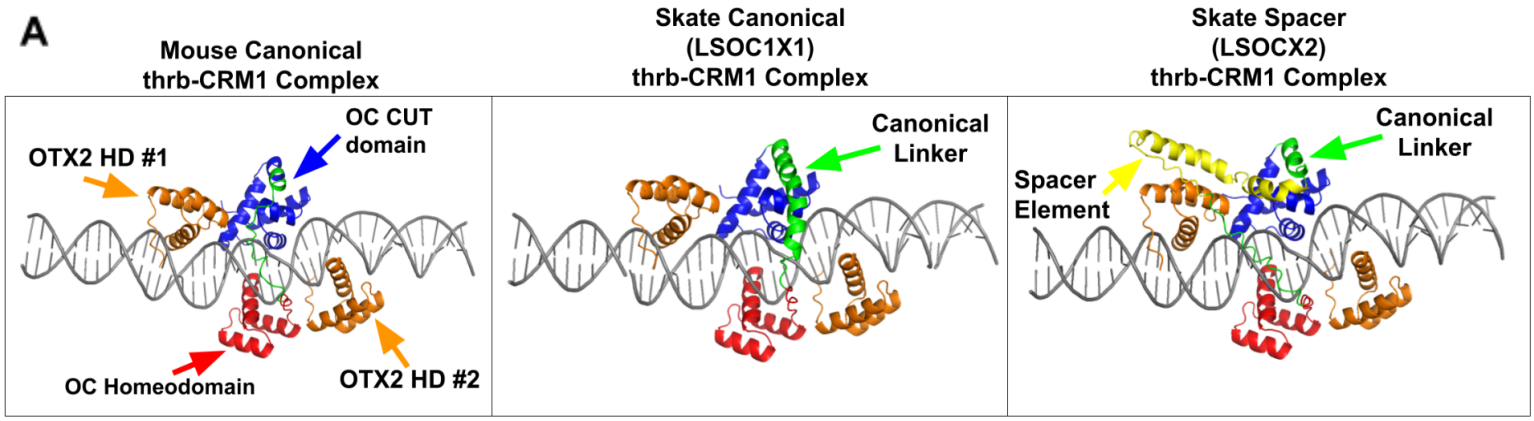
A
Mouse Canonical
thrb-CRM1 Complex
Skate Canonical
(LSOC1X1)
thrb-CRM1 Complex
Skate Spacer
(LSOCX2)
thrb-CRM1 Complex
OTX2 HD #1
OC CUT
domain
OC Homeodomain
OTX2 HD #2
Canonical
Linker
Spacer
Element
Canonical
Linker

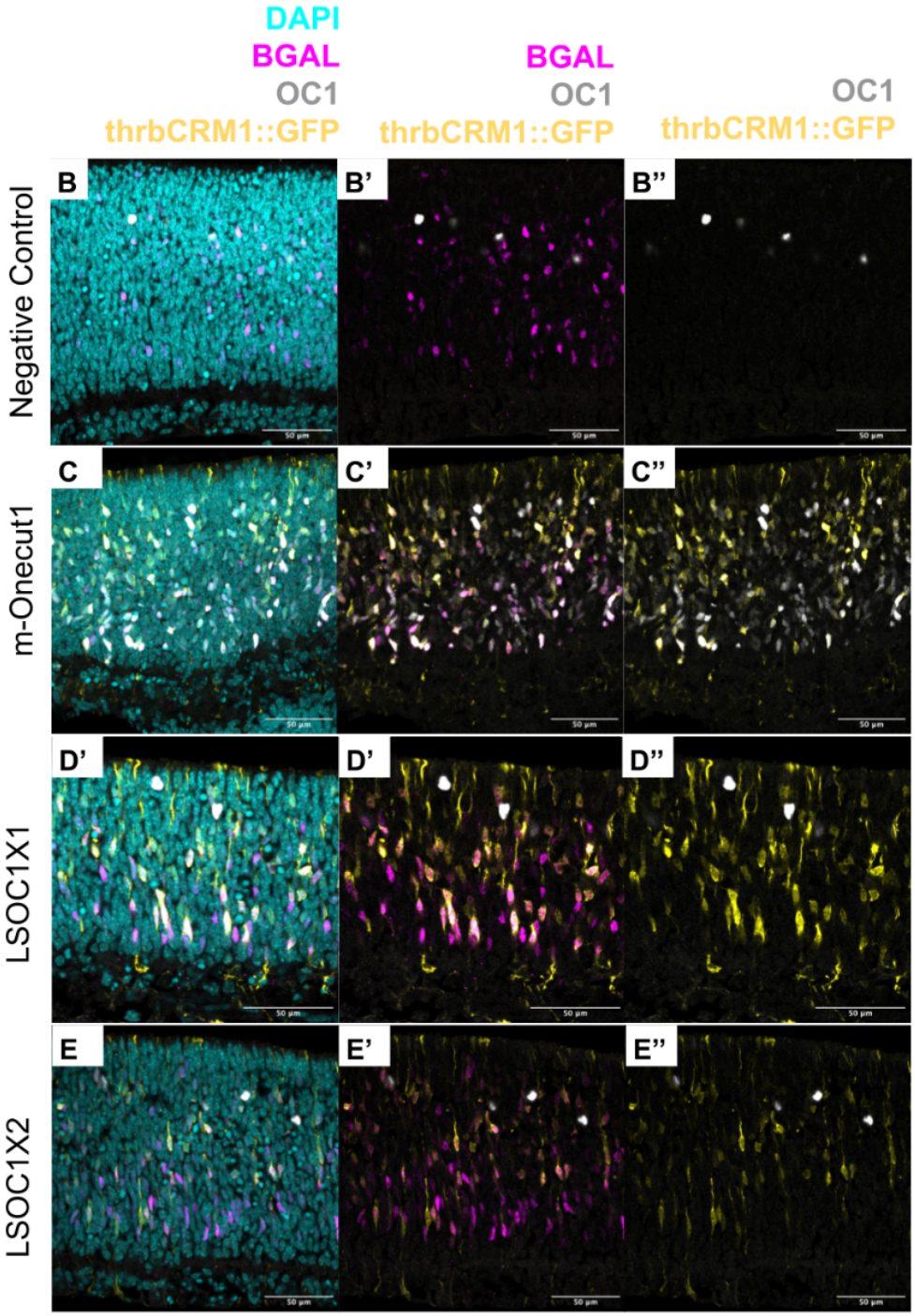
DAPI
BGAL
OC1
thrbCRM1::GFP
BGAL
OC1
thrbCRM1::GFP
OC1
thrbCRM1::GFP
Negative Control
m-Onecut1
LSOC1X1
LSOC1X2
B
B'
B''
C
C'
C''
D'
D'
D''
E
E'
E''